communications earth & environment

ARTICLE

https://doi.org/10.1038/s43247-023-00683-y OPEN

Arctic warming contributes to increase in Northeast Pacific marine heatwave days over the past decades

Se-Yong Song [1], Sang-Wook Yeh [1✉], Hyerim Kim [3] & Neil J. Holbrook [2,4]

The frequency and duration of marine heatwaves have been increasing with ocean warming due to climate change. In particular, the Northeast Pacific has experienced intense and extensive marine heatwaves since the late 1990s – characteristically called "the Blob". Here, an investigation of satellite-derived and reanalysis data supported by idealized coupled model experiments show that Arctic warming plays an important role in the increase in Northeast Pacific marine heatwave days during boreal summers. Strong Arctic warming has acted to change the atmospheric circulation pattern over the Northeast Pacific and reduce the low-level cloud fraction from late spring to early summer. We show that the enhancement of solar radiative heat fluxes and reduced latent heat loss over a relatively large area has favored an increase in sea surface temperatures and marine heatwave days. An idealized model experiment performed here, designed to isolate the impact of Arctic warming, supports this hypothesis. The projected changes of Arctic climate on the occurrence of marine heatwaves should be considered in climate change adaptation and mitigation plans.

[1] Department of Marine Sciences and Convergence Technology, Hanyang University, Ansan, South Korea. [2] Institute for Marine and Antarctic Studies, University of Tasmania, Hobart, Tasmania, Australia. [3] Institute of Cyber Security and Privacy, Korea University, Seoul, South Korea. [4] ARC Centre of Excellence for Climate Extremes, University of Tasmania, Hobart, Tasmania, Australia. ✉email: swyeh@hanyang.ac.kr

Marine heatwaves (MHWs) are prolonged extreme oceanic warm water events that can have profound impacts on marine ecosystems threatening marine biodiversity[1]. Reported impacts include mass bleaching of corals[2,3], high mortality rates of marine animals[4], and impacts to fisheries[5,6]. Several significant MHWs over the past 20 years have led to substantial impacts in the Mediterranean Sea in 2003[4,7], off Western Australia in 2011[8], the Northwest Atlantic in 2012[9], Tasman Sea in 2015/16[10], around northern Australia in 2016[11], and in the Northeast Pacific from 2013–2015[12,13], in 2019[14] and in 2020[15]. The properties of MHWs, including their frequency and duration, have been amplified due to anthropogenic warming[16], with these changes clearly detected in historical observations[17,18] and model projections under future climate change scenarios[19,20].

Due to the profound impacts associated with intense MHWs[1,21,22], understanding the mechanisms that lead to changes in MHWs is essential[23,24]. Important drivers of MHWs include local atmosphere-ocean coupled processes (producing net downward heat fluxes), warm ocean advection, and large-scale modes of climate variability, with atmospheric and/or oceanic teleconnections important when remotely forced[24]. In addition, a new driver, the Atlantic meridional overturning circulation, has been proposed in a recent study[25]. The Atlantic meridional overturning circulation slowdown will not only affect MHWs in the North Atlantic, but also affect those in the North Pacific via the hemispheric temperature contrast response. While long-term oceanic warming is the most important reason for changes in MHWs globally[17], there are notable differences in the mechanisms that affect regional MHW occurrences, intensity and duration[24].

The Northeast Pacific Ocean has experienced severe and broad-scale MHWs in recent years. Known iconically as "the Blob", recent characteristic Blob MHWs have been observed during the winters of 2013–14[12] and 2014–15[13], and the summers of 2014 and 2019[14]. These events have led to sometimes devastating impacts on sea life including the mortality of sea animals, critically reduced ocean primary productivity, and changes in biological species[12,26,27]. These Northeast Pacific MHWs have been attributed primarily to anomalously high sea level pressures associated with the North Pacific Oscillation (NPO)[28,29] as well as persistent low pressure anomalies in the Gulf of Alaska, which suppress heat loss from the ocean to atmosphere, causing extreme and prolonged warm sea surface temperature (SST) anomalies[12–14,30]. The associated reduction in surface winds and cloud cover has been identified as an important mechanism to explain summertime MHWs when marine stratocumulus clouds are otherwise typically most prevalent[14]. In addition, these overlying atmospheric conditions cause the shoaling of the ocean mixed layer, allowing excessive heat to distribute in a thin ocean mixed layer, leading to warm upper ocean temperature extremes in the Northeast Pacific[14,31].

Here, we explore the role of Arctic warming in increasing the number of MHW days experienced in the Northeast Pacific. The remarkable reduction in Arctic sea ice during the late spring and early summer since the late 1990s[32,33] has led to significant Arctic warming through increased local downward heat flux forcing and feedbacks[34]. Recent studies suggest that Arctic warming exerts a strong influence on mid-latitude extreme weather events by altering the atmospheric circulation patterns[35–38] including the NPO[39,40], albeit that the mechanisms are complex and debated[41–43]. In the present study, we provide observational and modeling evidence to show that accelerated Arctic warming acts to modify the North Pacific atmospheric circulation and has likely contributed to the recent increases in MHW days in the Northeast Pacific.

Results

Historical MHW properties in the Northeast Pacific. Figure 1a shows the spatial distribution of the average total number of MHW days per year (see "Methods" for MHW definition) in the Northeast Pacific from 1982 to 2019. In particular, the area-averaged total number of MHW days per year within the boxed region of the Northeast Pacific (32°−50°N, 132°−152°W, black box in Fig. 1a) is ~29 days with 7.4 days during summer (Fig. 1b).

The boreal summer (June-July-August, JJA) exhibits the largest significant upward trend in the number of MHW days since 1982 (average of 6.23 days decade^{-1}; Fig. 1c, e) compared to other seasons (Supplementary Fig. 1a–c). Similar to the upward trend in the box-averaged MHW days per year, the box-averaged SST during JJA also shows a significant upward trend in MHW days in the Northeast Pacific region (0.39 °C decade^{-1}; Fig. 1d, e) compared to other seasons (Supplementary Fig. 1d–f). The trend in the number of MHW days during spring (March-April-May) and autumn (September-October-November) could be partly explained by the increase in SST variability, which is known as the dominant driver for changes in MHW properties (Supplementary Fig. 2), and in contrast to that during JJA. Although MHW impacts will vary for different marine species depending on their ecological vulnerability and seasonality[44,45], summer MHWs might be expected to have larger ecological effects due to thermal tolerances exceeding those of other seasons[20]. We therefore focus our attention here on the total number of MHW days in the Northeast Pacific during JJA.

While there are some discrepancies in the spatial structure of climatological MHW days using different minimum duration thresholds (Supplementary Fig. 3), their hotspots of MHW days are very similar in spite of different minimum duration thresholds during JJA (Supplementary Fig. 3e–h) and annually (Supplementary Fig. 3a–d). The spatial pattern correlation coefficient (see "Methods") between the trends in mean SST and the MHW days (Fig. 1c, d) is 0.59 in the Northeast Pacific. The increased MHW days in recent decades, which resulted from the longer and more frequent MHWs, might be associated with increases in mean SST[17,18,46]. Our analysis also indicates that the time series of area-averaged SST (black box, Fig. 1d) is closely correlated with the MHW days during JJA over the period 1982–2019 ($r = 0.75$ detrended, where r is a simultaneous correlation coefficient, statistically significant at the 99% confidence level) (Fig. 1e). These results support the area-averaged SST variability including its upward trend—which may be due to natural variability, anthropogenic forcing, or their combined influences—being associated with the increased numbers of MHW days in the Northeast Pacific. In particular, the distinct SST warming trend in the Northeast Pacific (0.65 °C decade^{-1}) is statistically significant at the 95% confidence-level for the most recent 20-year period from 2000–2019, but not for the previous period from 1982–1999 (0.41 °C decade^{-1}). Indeed, the number of MHW days averaged over the Northeast Pacific (black box in Fig. 1) is about 2.2 and 12.1 days during the periods 1982–1999 and 2000–2019, respectively, and its difference is statistically significant at the 95% confidence-level. There are also distinct upward trends in MHW frequency, duration and intensity during JJA (Supplementary Fig. 4). In particular, the MHW days during JJA have significant correlation coefficients with their frequency ($r = 0.96$), duration ($r = 0.80$) and intensity ($r = 0.52$) over the period 1982–2019, and all correlation coefficients are statistically significant at the 95% confidence level. This demonstrates that the accelerated warming over the record is associated with the distinct increase in MHW days attributed to the longer and more frequent MHWs in the Northeast Pacific Ocean.

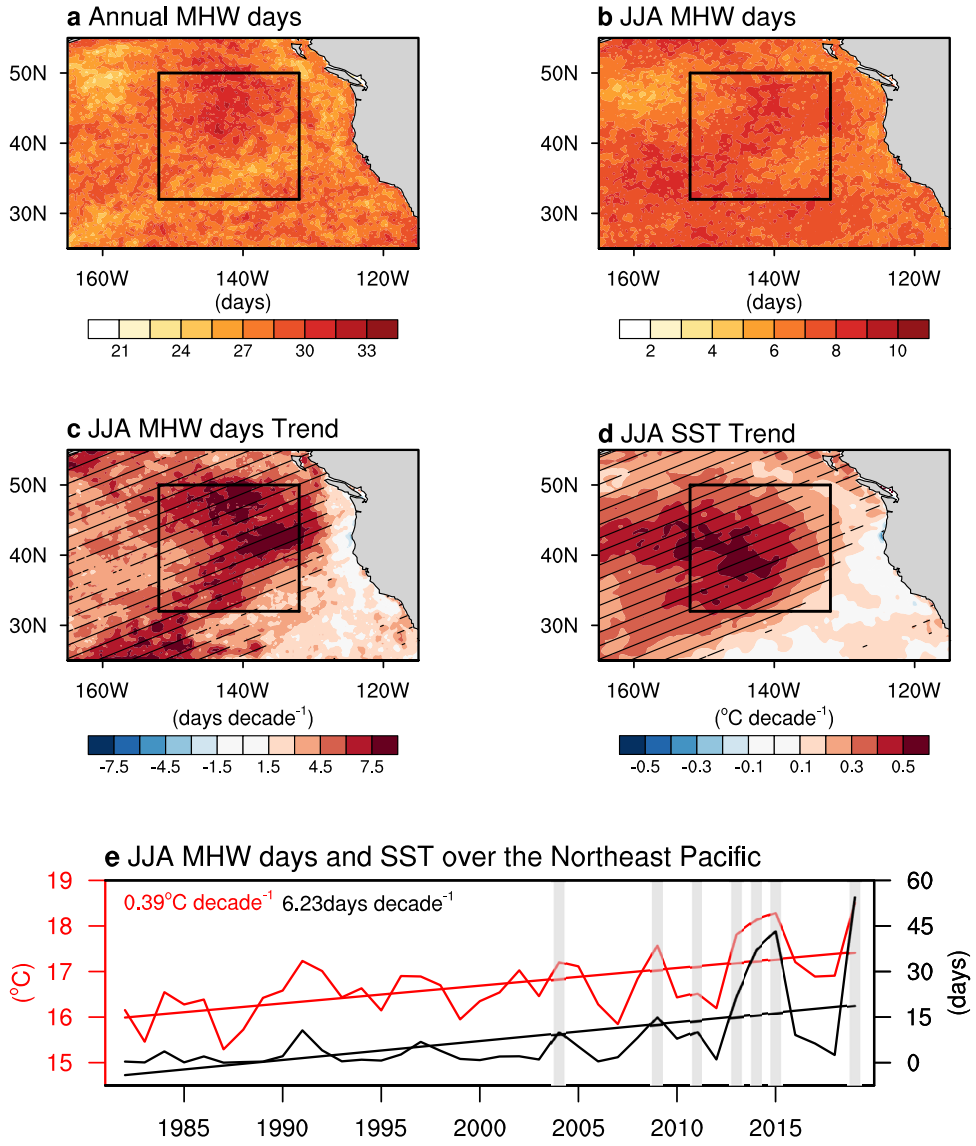

Fig. 1 Characteristics of the properties of MHWs and SST in the Northeast Pacific. Climatological distribution of **a** annual and **b** summer (June-July-August, JJA) count of MHW days (in days) for 1982–2019. Trend map of **c** MHW days (days decade^{-1}) and **d** SST (°C decade^{-1}) during JJA. Hatched regions in **c** and **d** indicate statistically significant values at the 90% confidence level based on a two-sided *t* test. The black box represents the area (32°–50°N, 132°–152°W) where SST and MHW days have been significantly increased. **e** Time series of mean SST (°C, red line) and MHW days (days, black line) during JJA averaged over the black box in **a**. Linear trends for 1982–2019 in each component are shown at the top left of the figure in **e**. Shade in gray in **e** denotes the years (2004, 2009, 2011, 2013, 2014, 2015, and 2019) when the MHW days during JJA were >10 days since the late 1990s.

Increases in MHW days and Arctic warming. In accordance with the accelerated Arctic warming and rapid decline in Arctic sea ice concentration since the late 1990s[32,33] (Supplementary Fig. 5), we hypothesized that the Arctic warming has led to the recent increases in SST and MHW days in the Northeast Pacific. To examine the effects of Arctic warming on the increased number of MHW days, we first selected the years since the late 1990s when the total number of MHW days during JJA is >10 days (2004, 2009, 2011, 2013, 2014, 2015, and 2019) (see "Methods"). We conducted a composite analysis based on sea ice concentration (SIC), sea level pressure (SLP) and low-level cloud cover (LCC) from the late spring to early summer (May-June-July, MJJ), respectively (Fig. 2). One month's lead time (i.e., MJJ) was found to be sufficient for SSTs to respond to the exchange of surface heat fluxes (Supplementary Tables 1, 2).

We find that the increase in MHW days during JJA is associated with a significant reduction in Arctic SIC during MJJ (Fig. 2a). This implies that there may exist connections of Arctic SIC during MJJ and the following atmospheric circulation in the Northeast Pacific with a lagged time. Atmospheric circulation patterns that lead to the increased MHW days are characterized by dipole-like SLP anomalies reminiscent of a positive phase of the NPO (+NPO) (Fig. 2b). A + NPO-like atmospheric circulation anomaly can induce anomalous easterly winds when the prevailing surface westerlies weaken. The resulting reduction in surface evaporation from the oceans causes anomalous surface layer warming by limiting latent heat loss from the ocean to the atmosphere (Supplementary Fig. 6). These processes are verified by significant correlations between the NPO index (see "Methods") and anomalous SSTs in the Northeast Pacific over the period 1982–2019 (Supplementary Table 1). Furthermore, this relationship becomes stronger during 2000–2019 than in the prior period from 1982–1999. Our further analysis indicates that a decrease in LCC during MJJ precedes the MHW event during

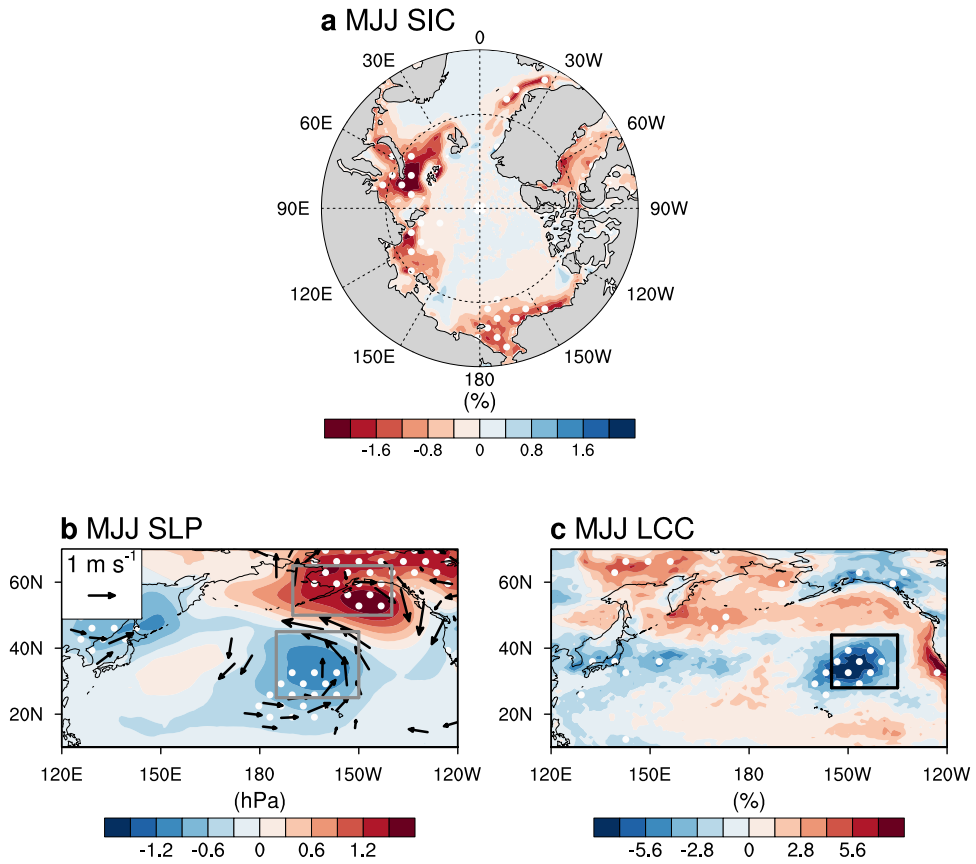

Fig. 2 Preceding conditions of sea ice concentration, atmospheric circulation and low-level cloud cover for the years of long MHW days. Composite map of **a** sea ice concentration (%), **b** sea level pressure (in hPa) and 850-hPa winds (m s^{-1}) and **c** low-level cloud cover (%) during May-June-July (MJJ) for the years (2004, 2009, 2011, 2013, 2014, 2015, and 2019) when the MHW days during JJA were >10 days since the late 1990s. The gray and black boxes in **b** and **c** represent definition for the NPO and LCC index, respectively (see "Methods"). Stippling regions in **b** and **c** indicate statistically significant values at the 90% confidence level based on a two-sided *t* test.

JJA (Fig. 2c). A decrease in LCC results in an increase in solar (shortwave) radiation reaching the ocean surface, leading to anomalous warming of the upper Northeast Pacific (Supplementary Fig. 7). These radiative effects induced by the low-level cloud cover are verified by a linear relationship between the LCC index (see "Methods") and anomalous SSTs in the Northeast Pacific (Supplementary Table 2).

While these surface heat fluxes locally drive the anomalous SST in the Northeast Pacific, MHW-favorable conditions appear to also be largely and remotely driven by the +NPO-like atmospheric circulation (Supplementary Figs. 6–8). Indeed, the peak of latent heat flux anomalies precedes the largest solar radiation anomalies by one month (Supplementary Fig. 8b, d). That is, the surface warming induced by the reduced latent heat loss acts to suppress the low-level cloud fraction along with the increase in shortwave radiation, maintaining the perturbed SST warming. This result implies that the +NPO-like atmospheric circulation is a primary driver of the increasing MHW days and the low-level cloud feedback has an important role in sustaining the MHWs in the Northeast Pacific similar to the prolonged 2019 summertime MHW event[14].

In addition, we found that trends in the atmospheric circulation are characterized by a +NPO-like SLP pattern along with a decreasing trend in LCCs over the period 1982–2019 (Fig. 3a, b). This suggests that the atmospheric circulation change toward a +NPO-like structure along with a decreasing trend of LCC contributes to the observed increases in MHW days in the Northeast Pacific in the recent past. Given that surface heat fluxes are closely linked to the atmospheric circulation over the North Pacific[47,48], the +NPO-like trend in atmospheric circulation may contribute to the upward trend in SSTs (Fig. 3c), comprising of an accelerated increase in SST after the late 1990s (0.65 °C $decade^{-1}$) compared with that before the late 1990s (0.41 °C $decade^{-1}$) (Fig. 3d). While correlation analysis does not indicate a cause-effect relationship, this result may imply that the +NPO-like trend in atmospheric circulation (Fig. 3a) is favorable to the increase in SSTs and the increased MHW days in the Northeast Pacific.

To verify this, we analyzed the probability distribution of daily Northeast Pacific SST anomalies, and specifically the changes in this distribution between the periods of 1982–1999 and 2000–2019. Note that the mean SST in the Northeast Pacific is 17.0 °C (16.4 °C) for the periods 2000–2019 (1982–1999), and their difference of 0.6 °C is statistically significant at the 99% confidence level (Fig. 3d). Notably, this distribution has shifted to a warmer state (Fig. 3e) and the right tail of the probability distribution shows a substantial increase in the warm extremes, in line with the increased MHW days since the late 1990s.

Model experiment. We hypothesized that the atmospheric circulation that characterizes a +NPO-like structure and the associated upward trend in the Northeast Pacific SSTs are attributable to the observed Arctic warming along with a rapid decline in Arctic SIC. To test this hypothesis, we conducted an idealized climate model experiment (Methods).

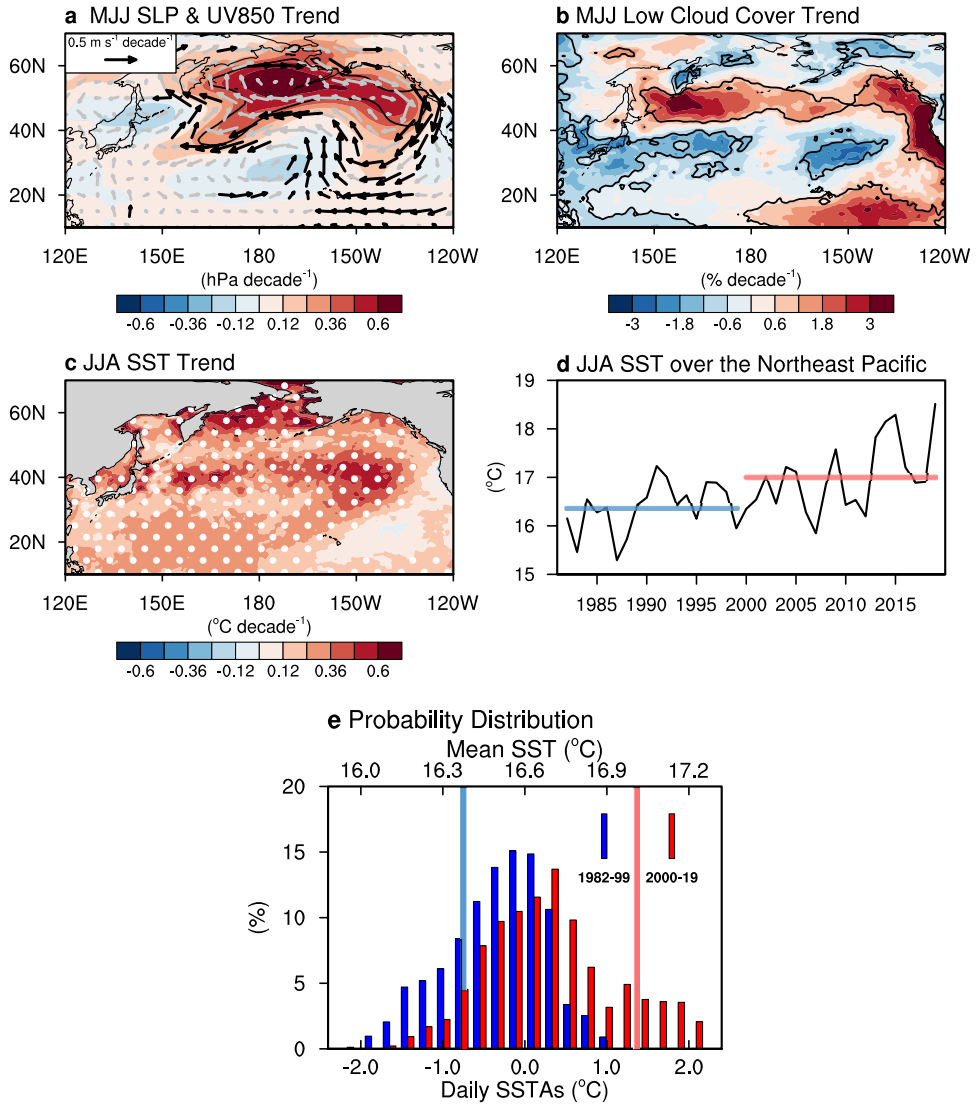

Fig. 3 Trends of atmospheric circulation, low-level cloud cover, SSTs and the probability distribution of daily SST obtained from reanalysis and observational-based datasets. Trend map of **a** SLP (hPa decade^{-1}) and 850-hPa winds (in m s^{-1} decade^{-1}), **b** LCC (% decade^{-1}) during MJJ and **c** SST (°C decade^{-1}) during JJA for 1982–2019. Black contour, vector and stippling regions in **a**–**c** indicate statistically significant values at the 90% confidence level based on a two-sided *t* test (all other vectors are shown in gray). **d** Time series of mean SST (°C, black line) during JJA in the Northeast Pacific. The light blue and red line in **d** denotes the mean SST values for 1982–1999 and 2000–2019, respectively. **e** Probability distribution of daily SST anomalies (SSTAs, °C on lower *x*-axis) in the Northeast Pacific during JJA for 1982–1999 (blue bar) and 2000–2019 (red bar) with their mean SST (°C on upper *x*-axis).

There is considerable agreement that CO_2 forcing is the main cause of SST warming globally. Here, we emphasize the role of Arctic warming in the Northeast Pacific Ocean. To isolate the Arctic warming, we restored the historical SST with a fixed CO_2 concentration in the Arctic region (north of 65ºN) as referred to ART_Exp. However, we do not exclude the role of greenhouse gas forcing because the Arctic warming is mainly due to the greenhouse gas forcing[49]. Such a model design has been used previously and successfully to isolate the impact of Arctic warming in previous studies[39,50]. We analyzed the simulated ensemble mean atmospheric and oceanic variables from 30 ensemble members by excluding internal variability to emphasize the role of Arctic sea-ice boundary forcing.

Similar to the observations, we found that the Arctic-forced atmospheric responses are characterized by a +NPO-like atmospheric circulation and a decreasing low-level cloud fraction from 1982–2019 (Fig. 4a, b). That is, the atmospheric circulation characteristic of a +NPO-like structure and decreasing low-level cloud fraction appears to play a key role in the simulated upward trend in SST over the Northeast Pacific (Fig. 4c). Concurrently, there is a distinct difference in mean SST between 2000–2019 and 1982–1999 (0.14 °C) in ART_Exp, which is statistically significant at the 99% confidence level (Fig. 4d). Furthermore, this result is verified by the overall warming shift of the probability distribution of daily SST anomalies simulated for each ensemble member between the last two decades of the 20th century and the first decades of the 21st century in ART_Exp (Fig. 4e). Hence, our model experiments demonstrate that Arctic warming related to sea ice loss provides a plausible attribution mechanism for the increases in MHW days.

It is noted that the magnitudes of trends in the ensemble mean response derived from the idealized model simulation (Fig. 4a–c) are smaller than those in the observations because the internal variability is reduced and the response to Arctic warming is isolated in the ensemble mean. In addition, the mean SST difference between ART_Exp and satellite-derived SST data

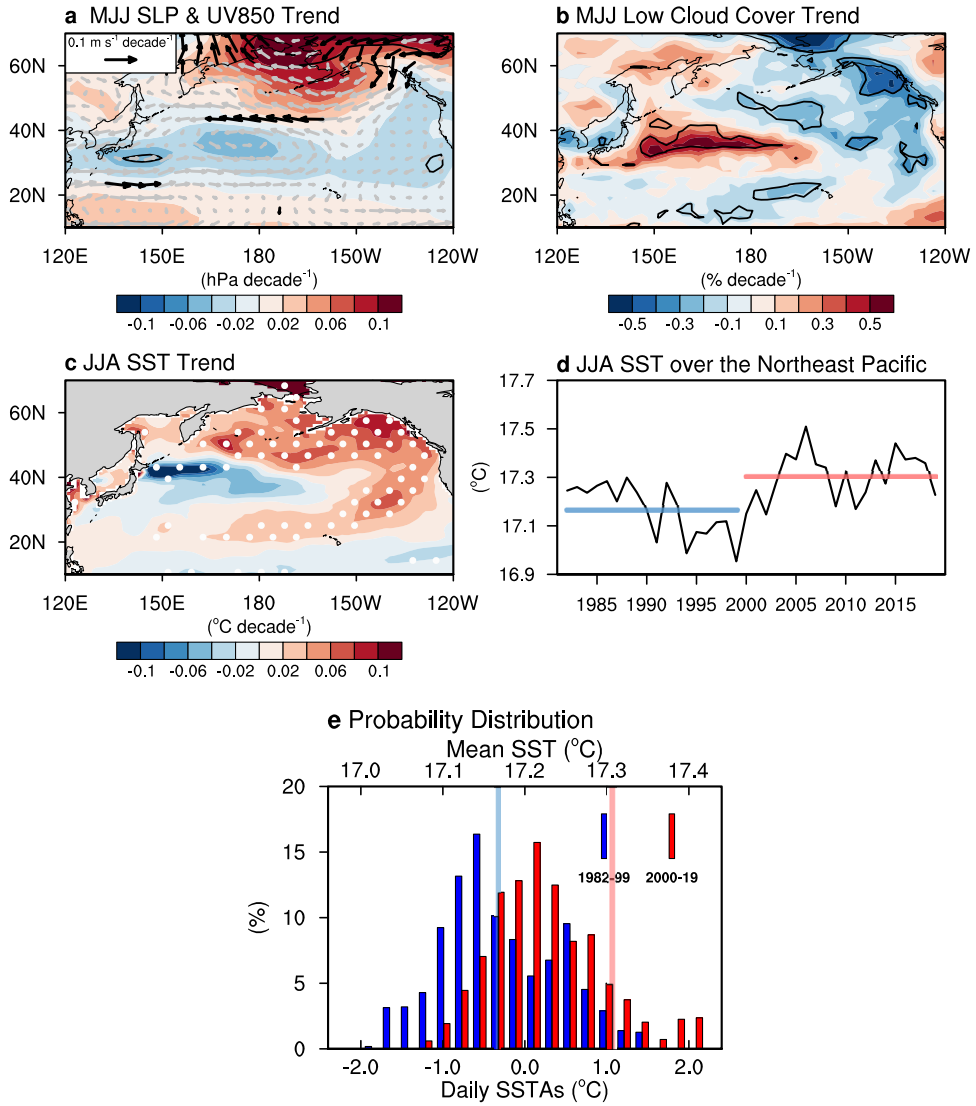

Fig. 4 Trends of atmospheric circulation, low-level cloud cover, SSTs and the probability distribution of daily SST simulated in ART_Exp. Trend map of **a** SLP (hPa decade^{-1}) and 850-hPa winds (m s^{-1} decade^{-1}), **b** LCC (% decade^{-1}) during MJJ and **c** SST (°C decade^{-1}) during JJA for 1982–2019. Black contour, vector and stippling regions in **a**–**c** indicate statistically significant values at the 90% confidence level based on a two-sided *t* test (all other vectors are shown in gray). **d** Time series of mean SST (°C, black line) during JJA in the Northeast Pacific. The light blue and red line in **d** denotes the mean SST values for 1982–1999 and 2000–2019, respectively. **e** Probability distribution of daily SSTAs (°C on lower *x*-axis) in the Northeast Pacific during JJA for 1982–1999 (blue bar) and 2000–2019 (red bar) with their mean SST (°C on upper *x*-axis).

during JJA is characterized by a cold (warm) bias in the western-to-central (eastern) North Pacific (Supplementary Fig. 9). This might act to underestimate (overestimate) MHW days in the west (east) of the Northeast Pacific.

Discussion

Remarkable MHWs occurred in the Northeast Pacific over the period 2013–15 and in 2019 (Fig. 1e). Those events were characterized by their distinct onset-to-decay mechanisms related to the large-scale ocean-atmosphere variability[13,14]. For example, the MHWs in 2013–15 and 2019 have been linked to SST variability in the tropical Pacific including El Niño–Southern Oscillation[13,14]. However, few studies have explored the role of atmospheric forcing from the high latitudes including the Arctic region on Northeast Pacific MHWs during the boreal summer. In the present study, we hypothesized that accelerated Arctic warming along with the diminished sea ice may act to drive the atmospheric circulation toward a +NPO-like structure and reduce the low-level cloud cover over the Northeast Pacific, providing conditions conducive to increase the number of MHW days during JJA. Along with changes in atmospheric circulation patterns, reduced latent heat loss and increased downward shortwave heat flux over the ocean may contribute to an increase in SST and MHW days in the Northeast Pacific.

Our idealized climate model experiment with 30 ensemble members supported the notion that the accelerated Arctic warming related to sea ice loss since the late 1990s significantly contributes to increase SST over the Northeast Pacific through the modulation of the atmospheric circulation patterns, resulting in an increase of MHW days there. However, there are notable differences between the observations and model simulations. For example, the atmospheric circulation pattern is more confined to high latitude (Fig. 4a), and the SST response is more shifted to the west coast of North America (Fig. 4c) in ART_Exp. Note that the CO_2 concentration is fixed at 353 ppm as the CO_2 concentration in 1989 in ART_Exp. This implies that a higher CO_2 concentration is prescribed during 1982–1988 than the observations. This might also be associated with a negative SST trend before

1989 (Fig. 4d). The ART_Exp is designed to isolate the impact of Arctic warming. In addition, the trend derived from observations might be influenced by other factors including CO_2 forcing and internal variability. While a single climate model experiment with a large ensemble is useful to isolate the forced response from internal variability[51,52], there are some issues regarding the required ensemble size and model dependency[51,53]. Thus, it would be useful in future to conduct the same simulations using different climate models with a large set of ensemble members. Nevertheless, we infer that the ongoing Arctic warming and further sea ice loss over the coming decades will further increase the MHW days in the Northeast Pacific. These projected changes are likely to pose further threats to marine ecosystems in this region without rapid and substantial global commitments and action to reduce carbon emissions together with the implementation of relevant climate change adaptation plans.

Methods

Observational-based SST and SIC data. Satellite-derived daily sea surface temperature (SST) data were obtained from the National Oceanic and Atmospheric Administration (NOAA) Optimum Interpolation (OI) SST v2.1[54]. These data were recently updated from the previous version of OISST v2[55], which has significantly improved the data quality since January 1, 2016. The NOAA OISST v2.1 is a 1/4° global gridded SST product based on Advanced Very High-Resolution Radiometer (AVHRR) infrared satellite data and in situ measurements (ships, buoys, and Argo float) with daily temporal coverage beginning in late 1981 to the present. For sea ice concentration (SIC), we used the monthly satellite SIC estimates from the Climate Data Record (CDR) provided by the NOAA National Snow and Ice Data Center (NSIDC)[56]. This SIC dataset provides a comprehensive Arctic SIC estimates since 1979 gridded on a polar stereographic projection with nominal 25 km × 25 km grid cells. Seasonal anomalies were derived by subtracting the climatological daily and monthly mean for 1982–2019 from the total mean field for the SST and SIC datasets, respectively.

Reanalysis atmospheric and heat flux data. The fifth generation of the European Centre for Medium-Range Weather Forecast (ECMWF) reanalysis product datasets (ERA5), with a horizontal resolution of 1°, was used for the atmospheric circulation and heat flux fields[57]. Although data errors and uncertainties may exist in the reanalysis datasets, among the available datasets for the present analysis period, the ERA5 data have been successfully implemented in previous studies of air-sea heat flux, low level cloud and large-scale climate variability in the North Pacific[58–60]. Seasonal anomalies were obtained by subtracting the climatological monthly mean for the period 1982–2019 from the total mean field.

Statistical significance test. To evaluate the statistical significance, we carry out the Student's *t* test with the effective degree of freedom due to serial correlation in the time series that given by the theoretical approximation[61,62].

Definition of a MHW event and composite years. We applied the now commonly used MHW definition[63] to detect MHWs in satellite-derived SST daily datasets (1/4° gridded) from NOAA OISST v2.1 for the period 1982–2019. MHWs were identified when daily SSTs were found to exceed the 90th percentile threshold above the seasonally varying daily climatology (baseline from 1982 to 2019) for at least five consecutive days. There is little change in the result when the 95th percentile threshold is used to detect a MHW event (Supplementary Fig. 10). For each MHW, we calculated its duration as the number of days from onset to end date. The duration of a single MHW event that crossed from one month to the next (one year to the next) is assigned to the month (year) when the event started. We then defined the MHW days as the total number of MHW days in each season and year. To identify favorable conditions for increased MHW days over the Northeast Pacific in recent decades, we performed the composite analyses for SST, SIC and low-level cloud cover (LCC).

The mean and one standard deviation for the MHW days during JJA were found to be 7.4 and 12.3 days, respectively. We selected the years since the late 1990s when the MHW days during JJA were above 10 days. The large temporal variance for MHW days (i.e., 12.3 day) makes it difficult to select the composite threshold. The 10 days are basically obtained from the composite thresholds based on the SST averaged over the Northeast Pacific (32°–50°N, 132°–152°W, box in Fig. 1). The mean SST averaged over the Northeast Pacific during JJA is 16.7 °C and one standard deviation is 0.71 °C. The years >0.7 standard deviation (0.5 °C) from its mean are 1991, 2004, 2009, 2013, 2014, 2015 and 2019, which are almost identical with the years when the total number of MHW days during JJA is >10 days since the late 1990s (2004, 2009, 2011, 2013, 2014, 2015, and 2019). For convenience, we use the composite threshold based on MHW days (i.e., 10 days), not the SST. In fact, 10 days is the closest threshold following the mean SST mentioned above. Note that the main results in the present study are not sensitive to the choice of the composite threshold including the 75th percentile of the interquartile range. Meanwhile, there is some discussion about the spatial and temporal scale for MHW detection[44]. We further examined the sensitivity to the MHW detection using various thresholds of minimum duration including 10-days, 20-days, and 30-days (Supplementary Fig. 3). The spatial structures of climatological MHW days with different thresholds are similar over the Northeast Pacific (Supplementary Fig. 3a–h). Furthermore, there are distinct MHW trend patterns and temporal evolutions consistent with those based on the 5-day threshold MHW detection metrics (Supplementary Fig. 3i–m). The composite years with peaks for MHW days also show little change.

North Pacific Oscillation index. To quantify the NPO variability, we defined the NPO index as the difference in SLP anomalies between the northern (50°−65°N, 140°−170°W) and southern (25°−45°N, 150°−175°W) lobe of the North Pacific region, as shown in Fig. 2b. The NPO index shows a positive linear trend for the present analysis period (Supplementary Fig. 11a) and there is a strong interannual relationship between this index and SST over the Northeast Pacific (Supplementary Table 1).

Low-level cloud cover index. The LCC index was calculated as the LCC anomalies averaged over (28°−44°N, 135°−155°W), as shown in Fig. 2c. It displays a negative linear trend (Supplementary Fig. 11b) and a tight connection with SST over the Northeast Pacific (Supplementary Table 2).

Spatial pattern correlation. To measure how similar the mean SST and MHW days trend patterns are over the Northeast Pacific (25°−55°N, 115°−165°W), we estimated the spatial pattern correlation coefficient. We calculated the centered pattern correlation coefficient between paired spatial patterns weighted by the cosine of latitude.

Model experiment. We performed idealized coupled general circulation model experiments using the GFDL CM2.1[64]. The horizontal resolutions of the atmosphere and land were 2° latitude and 2.5° longitude, with 24 atmospheric levels. The ice-ocean model was composed of a 200-latitude and 360-longitude tripolar grid with 50 oceanic vertical levels. To investigate the impact of Arctic warming, the SSTs in the high latitudes (north of 65°N) were restored to the linearly interpolated historical observed daily SST for the period 1951–2019. The experiment consisted of 30 ensemble members with different initial atmospheric and oceanic conditions. Note that the CO_2 concentration, which is known to be one of the major contributors to the long-term SST trend, is fixed at 353 ppm as the CO_2 concentration in 1989.

Specifically, the historical SST was restored in the Arctic region with a five-day restoring time scale. The SIC simulated in this model mostly follows the observational evolution (Supplementary Figs. 5, 12), implying that sea ice rapidly adjusts to the SST evolution because the simulated SIC was thermodynamically balanced with the restored SST in the Arctic. In addition, the ocean model was fully coupled with the atmosphere and sea ice models outside of the SST restoring region. This model experimental configuration has been previously used to explore the impact of Arctic warming in previous studies[39,50]. For example, the simulations used in this study are the same as those undertaken by Kim et al.[39] that investigated the connection between Arctic sea ice loss and the occurrence of Central Pacific El Niño events. It is noteworthy that we performed the additional 15 ensemble member simulations with an extended integration period in the present study to more rigorously isolate the forced response from internal variability. That is, these idealized experiments were designed to identify whether Arctic warming related to sea ice loss, which is known to be strongly due to anthropogenic climate change[49], could contribute to the atmospheric circulation over the North Pacific in association with the increases in MHW days. In particular, we used ensemble mean variables from each of 30 ensemble members in CO_2 fixed simulations to emphasize the response of the Arctic warming related to sea ice loss by minimizing the impact of internal variability and greenhouse-gas forcing in other non-Arctic parts of the climate system. Seasonal anomalies were derived by subtracting the climatological daily and monthly mean for the period 1982–2019 from the total mean field for SST and all other variables, respectively.

Data availability

The OISSTv2.1 (ref. [54]) data set is available from the NOAA Physical Sciences Laboratory website (https://psl.noaa.gov/data/gridded/data.noaa.oisst.v2.highres.html). The satellite SIC (ref. [56]) data set is available from the NSIDC website (http://nsidc.org/data/nsidc-0051.html). The ERA5 (ref. [57]) data set is available from the ECMWF website (https://www.ecmwf.int/en/forecasts/datasets/reanalysis-datasets/era5). The GFDL CM2.1 model and corresponding data are available from the GFDL portal server (https://nomads.gfdl.noaa.gov/CM2.X).

Code availability

Codes used to generate main figures are available on request from the author (sysong619@gmail.com).

Received: 14 April 2022; Accepted: 12 January 2023;
Published online: 07 February 2023

References

1. Smale, D. A. et al. Marine heatwaves threaten global biodiversity and the provision of ecosystem services. *Nat. Clim. Change* **9**, 306–312 (2019).
2. Hughes, T. P. et al. Global warming and recurrent mass bleaching of corals. *Nature* **543**, 373–377 (2017).
3. McWilliams, J. P., Côté, I. M., Gill, J. A., Sutherland, W. J. & Watkinson, A. R. Accelerating impacts of temperature-induced coral bleaching in the Caribbean. *Ecology* **86**, 2055–2060 (2005).
4. Garrabou, J. et al. Mass mortality in Northwestern Mediterranean rocky benthic communities: effects of the 2003 heat wave. *Glob. Change Biol.* **15**, 1090–1103 (2009).
5. Cheung, W. W. & Frölicher, T. L. Marine heatwaves exacerbate climate change impacts for fisheries in the northeast Pacific. *Sci. Rep.* **10**, 1–10 (2020).
6. Pershing, A. J. et al. Slow adaptation in the face of rapid warming leads to collapse of the Gulf of Maine cod fishery. *Science* **350**, 809–812 (2015).
7. Olita, A. et al. Effects of the 2003 European heatwave on the Central Mediterranean Sea: surface fluxes and the dynamical response. *Ocean Sci.* **3**, 273–289 (2007).
8. Pearce, A. F. & Feng, M. The rise and fall of the "marine heat wave" off Western Australia during the summer of 2010/2011. *J. Mar. Syst.* **111**, 139–156 (2013).
9. Chen, K., Gawarkiewicz, G. G., Lentz, S. J. & Bane, J. M. Diagnosing the warming of the Northeastern US Coastal Ocean in 2012: a linkage between the atmospheric jet stream variability and ocean response. *J. Geophys. Res.: Oceans* **119**, 218–227 (2014).
10. Oliver, E. C. et al. The unprecedented 2015/16 Tasman Sea marine heatwave. *Nat. Commun.* **8**, 1–12 (2017).
11. Benthuysen, J. A., Oliver, E. C., Feng, M. & Marshall, A. G. Extreme marine warming across tropical Australia during austral summer 2015–2016. *J. Geophys. Res.: Oceans* **123**, 1301–1326 (2018).
12. Bond, N. A., Cronin, M. F., Freeland, H. & Mantua, N. Causes and impacts of the 2014 warm anomaly in the NE Pacific. *Geophys. Res. Lett.* **42**, 3414–3420 (2015).
13. Di Lorenzo, E. & Mantua, N. Multi-year persistence of the 2014/15 North Pacific marine heatwave. *Nat. Clim. Change* **6**, 1042–1047 (2016).
14. Amaya, D. J., Miller, A. J., Xie, S.-P. & Kosaka, Y. Physical drivers of the summer 2019 North Pacific marine heatwave. *Nat. Commun.* **11**, 1–9 (2020).
15. Chen, Z., Shi, J., Liu, Q., Chen, H. & Li, C. A persistent and intense marine heatwave in the Northeast Pacific during 2019–2020. *Geophys. Res. Lett.* **48**, e2021GL093239 (2021).
16. Laufkötter, C., Zscheischler, J. & Frölicher, T. L. High-impact marine heatwaves attributable to human-induced global warming. *Science* **369**, 1621–1625 (2020).
17. Oliver, E. C. Mean warming not variability drives marine heatwave trends. *Clim. Dyn.* **53**, 1653–1659 (2019).
18. Oliver, E. C. et al. Longer and more frequent marine heatwaves over the past century. *Nat. Commun.* **9**, 1–12 (2018).
19. Frölicher, T. L., Fischer, E. M. & Gruber, N. Marine heatwaves under global warming. *Nature* **560**, 360–364 (2018).
20. Oliver, E. C. et al. Projected marine heatwaves in the 21st century and the potential for ecological impact. *Front. Mar. Sci.* **6**, 734 (2019).
21. Smith, K. E. et al. Biological Impacts of Marine Heatwaves. *Annu. Rev. Mar. Sci.* **15**, 119–145 (2022).
22. Smith, K. E. et al. Socioeconomic impacts of marine heatwaves: Global issues and opportunities. *Science* **374**, eabj3593 (2021).
23. Holbrook, N. J. et al. Keeping pace with marine heatwaves. *Nat. Rev. Earth Environ.* **1**, 482–493 (2020).
24. Holbrook, N. J. et al. A global assessment of marine heatwaves and their drivers. *Nat. Commun.* **10**, 1–13 (2019).
25. Ren, X. & Liu, W. The role of a weakened Atlantic meridional overturning circulation in modulating marine heatwaves in a warming climate. *Geophys. Res. Lett.* **48**, e2021GL095941 (2021).
26. Cavole, L. M. et al. Biological impacts of the 2013–2015 warm-water anomaly in the Northeast Pacific: winners, losers, and the future. *Oceanography* **29**, 273–285 (2016).
27. Kintisch, E. 'The Blob' invades Pacific, flummoxing climate experts. *Science* **348**, 17–18 (2015).
28. Rogers, J. C. The north Pacific oscillation. *J. Clim.* **1**, 39–57 (1981).
29. Walker, G. & Bliss, E. Memoirs of the royal meteorological society. *World Weather V* **4**, 53–84 (1932).
30. Johnstone, J. A. & Mantua, N. J. Atmospheric controls on northeast Pacific temperature variability and change, 1900–2012. *Proc. Natl Acad. Sci. USA* **111**, 14360–14365 (2014).
31. Amaya, D. J. et al. Are long-term changes in mixed layer depth influencing North Pacific marine heatwaves? *Bull. Am. Meteorol. Soc.* **102**, S59–S66 (2021).
32. Serreze, M. C. & Stroeve, J. Arctic sea ice trends, variability and implications for seasonal ice forecasting. *Philos. Trans. R. Soc. A: Math. Phys. Eng. Sci.* **373**, 20140159 (2015).
33. Comiso. J. C., Parkinson, C. L., Gersten, R. & Stock, L. Accelerated decline in the Arctic sea ice cover. *Geophys. Res. Lett.* **35**, L01703 (2008).
34. Stuecker, M. F. et al. Polar amplification dominated by local forcing and feedbacks. *Nat. Clim. Change* **8**, 1076–1081 (2018).
35. Cohen, J. et al. Recent Arctic amplification and extreme mid-latitude weather. *Nat. Geosci.* **7**, 627–637 (2014).
36. Francis, J. A. & Vavrus, S. J. Evidence linking Arctic amplification to extreme weather in mid-latitudes. *Geophys. Res. Lett.* **39**, L06801 (2012).
37. Overland, J. E. et al. Nonlinear response of mid-latitude weather to the changing Arctic. *Nat. Clim. Change* **6**, 992–999 (2016).
38. Screen, J. A., Simmonds, I., Deser, C. & Tomas, R. The atmospheric response to three decades of observed Arctic sea ice loss. *J. Clim.* **26**, 1230–1248 (2013).
39. Kim, H. et al. Arctic sea ice loss as a potential trigger for Central Pacific El Niño events. *Geophys. Res. Lett.* **47**, e2020GL087028 (2020).
40. Yeo, S.-R. et al. Recent climate variation in the Bering and Chukchi Seas and its linkages to large-scale circulation in the Pacific. *Clim. Dyn.* **42**, 2423–2437 (2014).
41. Cohen, J. et al. Divergent consensuses on Arctic amplification influence on midlatitude severe winter weather. *Nat. Clim. Change* **10**, 20–29 (2020).
42. Blackport, R. & Screen, J. A. Weakened evidence for mid-latitude impacts of Arctic warming. *Nat. Clim. Change* **10**, 1065–1066 (2020).
43. Dai, A. & Song, M. Little influence of Arctic amplification on mid-latitude climate. *Nat. Clim. Change* **10**, 231–237 (2020).
44. Jacox, M. G., Alexander, M. A., Bograd, S. J. & Scott, J. D. Thermal displacement by marine heatwaves. *Nature* **584**, 82–86 (2020).
45. Atkinson, J., King, N. G., Wilmes, S. B. & Moore, P. J. Summer and winter marine heatwaves favor an invasive over native seaweeds. *J. Phycol.* **56**, 1591–1600 (2020).
46. Frölicher, T. L. & Laufkötter, C. Emerging risks from marine heat waves. *Nat. Commun.* **9**, 1–4 (2018).
47. Alexander, M. A. & Scott, J. D. Surface flux variability over the North Pacific and North Atlantic oceans. *J. Clim.* **10**, 2963–2978 (1997).
48. Cayan, D. R. Variability of latent and sensible heat fluxes estimated using bulk formulae. *Atmos.-Ocean* **30**, 1–42 (1992).
49. Gillett, N. P. et al. Attribution of polar warming to human influence. *Nat. Geosci.* **1**, 750–754 (2008).
50. Kug, J.-S. et al. Two distinct influences of Arctic warming on cold winters over North America and East Asia. *Nat. Geosci.* **8**, 759–762 (2015).
51. Deser, C., Phillips, A., Bourdette, V. & Teng, H. Uncertainty in climate change projections: the role of internal variability. *Clim. Dyn.* **38**, 527–546 (2012).
52. Kay, J. E. et al. The Community Earth System Model (CESM) large ensemble project: a community resource for studying climate change in the presence of internal climate variability. *Bull. Am. Meteorol. Soc.* **96**, 1333–1349 (2015).
53. Milinski, S., Maher, N. & Olonscheck, D. How large does a large ensemble need to be? *Earth Syst. Dyn.* **11**, 885–901 (2020).
54. Huang, B. et al. Improvements of the daily optimum interpolation sea surface temperature (DOISST) version 2.1. *J. Clim.* **34**, 2923–2939 (2021).
55. Reynolds, R. W. et al. Daily high-resolution-blended analyses for sea surface temperature. *J. Clim.* **20**, 5473–5496 (2007).
56. Peng, G., Meier, W. N., Scott, D. & Savoie, M. A long-term and reproducible passive microwave sea ice concentration data record for climate studies and monitoring. *Earth Syst. Sci. Data* **5**, 311–318 (2013).
57. Hersbach, H. et al. The ERA5 global reanalysis. *Q. J. R. Meteorol. Soc.* **146**, 1999–2049 (2020).
58. Fu, H., Zhan, R., Wu, Z., Wang, Y. & Zhao, J. How does the Arctic Sea ice affect the interannual variability of tropical cyclone activity over the Western North Pacific? *Front. Earth Sci.* **9**, 331 (2021).
59. Blossey, P. N., Bretherton, C. S. & Mohrmann, J. Simulating observed cloud transitions in the northeast Pacific during CSET. *Monthly Weather Rev.* **149**, 2633–2658 (2021).
60. Gupta, A. S. et al. Drivers and impacts of the most extreme marine heatwave events. *Sci. Rep.* **10**, 1–15 (2020).
61. Zwiers, F. W. & Von Storch, H. Taking serial correlation into account in tests of the mean. *J. Clim.* **8**, 336–351 (1995).
62. Bretherton, C. S., Widmann, M., Dymnikov, V. P., Wallace, J. M. & Bladé, I. The effective number of spatial degrees of freedom of a time-varying field. *J. Clim.* **12**, 1990–2009 (1999).
63. Hobday, A. J. et al. A hierarchical approach to defining marine heatwaves. *Prog. Oceanogr.* **141**, 227–238 (2016).
64. Delworth, T. L. et al. GFDL's CM2 global coupled climate models. Part I: Formulation and simulation characteristics. *J. Clim.* **19**, 643–674 (2006).

Acknowledgements
The authors acknowledge the valuable comments from three anonymous reviewers that significantly improved this manuscript. This work was funded by the project "Investigation and prediction system development of marine heatwave around the Korean Peninsula originated from the subarctic and western Pacific (20190344)" from the Ministry of Oceans and Fisheries, Korea. NJH acknowledges funding from the ARC Centre of Excellence for Climate Extremes (CE170100023).

Author contributions
S.-Y.S. and S.-W.Y. proposed and conceived the study. S.-Y.S. and H.R.K. conducted the analysis and model experiments. S.-Y.S. and S.-W.Y. wrote the initial draft of the paper. N.J.H. contributed to interpreting the analysis results and revising the paper.

Competing interests
The authors declare no competing interests.

Additional information
Supplementary information The online version contains supplementary material available at https://doi.org/10.1038/s43247-023-00683-y.

Correspondence and requests for materials should be addressed to Sang-Wook Yeh.

Peer review information *Communications Earth & Environment* thanks Shuo Wang, Zhenya Song and the other, anonymous, reviewer(s) for their contribution to the peer review of this work. Primary Handling Editor: Heike Langenberg. Peer reviewer reports are available.